Supporting information for: Microscopic Symmetry Imposed by Rotational Symmetry Boundary Conditions in Molecular Dynamics Simulation

Amitava Roy and Carol Beth Post*

E-mail: cbp@purdue.edu

1 Rotational Symmetry Boundary Condition (RSBC)

Periodicity treated implicitly determines nonbonded interaction using the minimum image convention:

$$\acute{V_a} = V_a - nearint[V_a/L_a] \cdot L_a, \tag{1}$$

where V_a and $\acute{V_a}$ are component of distance vectors, L_a is the length of the periodic box along V_a, and $nearint[...]$ is nearest integer value of $[...]$. Application of Eq. (1) to relative distances in an infinite periodic system allows selection of the closest copy of replicated atoms for determining the nonbonded interactions in open crystallographic space group symmetry. Self-image interactions are avoided with an appropriate sized primary unit. With closed point group symmetry and rotational symmetry boundary conditions (RSBC), it is not possible to utilize the minimum image convention or to avoid self-image and replicate-image interactions near certain rotational symmetry axes. A subset of the 60 icosahedral symmetry operators is needed to generate the full capsid from a pentameric primary unit. The choice of the subset can be optimized to minimize, but not avoid, the self-image and replicate-image interactions.

*To whom correspondence should be addressed

The choice for the subset of icosahedral symmetry operators must meet two criteria:[1]

1. In explicit treatment of image atoms, when primary atoms cross a wall of the primary cell, their coordinates are transformed back into the primary cell using inverse of one of the image operators. This procedure is called re-centering. To avoid a discontinuity in energy, re-centering must move the atom to the identical micro-environment, with equivalent nonbonded interactions for primary and image atoms as existed before re-centering. Re-centering is essential for implementation of a general symmetry boundary condition because of the explicit treatment of image atoms. Without re-centering, water molecules that leave the primary cell will interact with an increasing number of image atoms leading to a corresponding increase in the nonbonded pair list. As a result, the total energy of the system decreases over time (data not shown here).

2. Each symmetry operator must have its inverse operator in the listed subset of operators. This requirement of the IMAGE facility of CHARMM is imposed for computational efficiency in calculating energies.[2] Fulfillment of the first criterion guarantees fulfillment of this criterion for the subset of icosahedral symmetry operators used in this article.

A subset of the icosahedral symmetry operators (Table 1) was selected to transform the primary coordinates to image coordinates. For the five nearest neighbor units positioned at the pentamer edges of the primary unit the symmetry operators were selected such that symmetrical forces were imposed at some but not all rotational axes. The five operators of each row of Table 1 transform an asymmetric unit, or protomer of a virus, to a pentameric unit. Assuming the top-row operators form the pentamer of the primary unit, one operator of each row 2-12 is needed to complete an icosahedron. We limit our attention to generating images of only neighboring pentamers given that the pentamer size is greater than the nonbonded cutoff distance. Operators in bold face in rows 2, 5, 6, 9, and 11 of Table 1 generate these neighboring pentamers. The only set of operators, one from each of these rows, that satisfies the two conditions for the IMAGE facility enumerated above are the operators Z (row 2), F_1ZF_3 (row 5), ZF_1ZF_3 (row 6), F_2ZF_4 (row 9), and XF_2ZF_4

(row 11). The set contains the inverse of each operator; the Z transformation is self-inverse, while F_1ZF_3/F_2ZF_4 and ZF_1ZF_3/XF_2ZF_4 are inverse transformations. That the first condition is satisfied can be determined from Figure 1a, which shows in a two-dimensional projection the primary unit and five nearest-neighbor image units generated with this choice of icosahedral operators. Recall that, because the pentamer is the primary simulation set, each pentameric corner, labeled A through E, is distinct from the other corners. An atom leaving primary unit near 3f1, as shown in Figure 1a, will be re-centered near 3f4. Before leaving the primary unit atom was interacting with primary atoms near corner A and images of atoms near corner B and D. After re-centering the atom will interact with primary atoms near corner D and images of atoms near corner A and B. Thus re-centering of atoms that move into an image region returns the atom to the exact environment within the primary unit. Similarly an atom near 3f3 leaving primary unit will be re-centered near 3f3. Figure 1b show two-dimensional projection of primary unit and five nearest-neighbor image units generated with symmetry operators underlined in Table 1 which do not satisfy the first criterion mentioned above. An atom leaving primary unit near 3f1 in Figure 1b, where micro-environment generated by corners A, B & E, will be re-centered near 3f2 where the micro-environment is different and generated by corners A, B & D. Simulation can not be performed with such a set of symmetry operators as energy will be discontinuous after re-centering.

Figure 1a showing the primary pentameric unit of the icosahedron and illustrates the failure at certain axes of rotational symmetry of the minimum image convention used for generating non-bonded list under periodic boundary conditions. Clearly this algorithm fails near axes *2f1*, *3f3* and *3f5* as explained in section 2.2 of article. Near other symmetry axes images are not positioned near the primary unit guarantees avoidance of replicate-image and self-image interactions. For example near axes 3f1 of Figure 1a atoms near $\angle EAB$ interacts with atoms near $\angle C'D'E'$ and $\angle A'B'C'$ of image units and avoid self-image and replicate-image interactions. In spite of violations of minimum image convention near certain symmetry axes, RSBC are properly handled by explicit treatment of image atoms with the limitation that the resulting interactions impose microscopic symmetry of forces for a small number of nonbonded pairs.

At the 2-fold symmetry axis *2f1*, and 3-fold symmetry axes *3f3* and *3f5* (Figure 1a) microscopic symmetry is imposed by forces from self-image interactions and from interactions with replicate primary and image atoms located near the axes. Other 2-fold, 3-fold, and of course, the 5-fold icosahedral symmetry axes are microscopically asymmetric given that primary and image atoms are not replicated and all nonbonded interactions are with independent atoms.

2 Convergence

Properties investigated in this article depend on magnitude of V_{rms} and the density of atoms within a shell of different thickness near a symmetry axis.

$$V_{rms} \equiv \sqrt{\frac{\sum_{i=1}^{n} m_i v_i^2}{\sum_{i=1}^{n} m_i}} \tag{2}$$

where n is number of atoms and m_i and v_i are mass and magnitude of velocity of ith atom.

Instantaneous temperature the system depends on V_{rms}.

$$T(t) = \sum_{i=1}^{N} \frac{m_i v_i^2(t)}{k_B N_f} \tag{3}$$

where N is total number of atom in the system, N_f id number of degrees of freedom and k_B is Boltzmann's constant.

In Figure 2a temperature of solvated viral capsid during 2 ns production time of simulation is shown. Densities of heavy atoms of viral capsid within cylindrical shells of 1 Å width around 3-fold symmetry axis 3f1 are shown in Figure 2b. Densities are shown for shell at 3 different distances with their midpoints at 5 Å (red), 7 Å (green) and 9 Å (blue). Both temperature and densities of heavy atom are well converged during the simulation.

In Figure 3 the distribution of the main chain ϕ, ψ dihedral angles are shown for the residues 117 of VP2, and 122 and 199 of VP3 in Figure 3 for four additional sets of 2 ns production time of simulation. These Ramachandran plots reveal that the distributions for these residues positioned

near the 3f1, 3f2 or 3f4 axes (panel a,c and e in Figure 3) do not differ from those at *3f3* or *3f5* axes (panel b,d and f in Figure 3). In 5 different independent simulations the ϕ, ψ dihedral angles spans similar area in Ramachandran plots which indicates that in 2 ns of production time lowest energy regions of underlying energy surface are well populated.

References

(1) Brooks B.R., C.L. Brooks 3rd, A.D. Mackerell Jr, L. Nilsson, R.J. Petrella, B. Roux, Y. Won, G. Archontis, C. Bartels, S. Boresch, A. Caflisch, L. Caves, Q. Cui, A.R. Dinner, M. Feig, S. Fischer, J. Gao, M. Hodoscek, W. Im, K. Kuczera, T. Lazaridis, J. Ma, V. Ovchinnikov, E. Paci, R.W. Pastor, C.B. Post, J.Z. Pu, M. Schaefer, B. Tidor, R.M. Venable, H.L. Woodcock, X. Wu, W. Yang, D.M. York, and M. Karplus *J. Comput. Chem.*, **30, 2009**, 1545–1614.

(2) R. Brooks B., R. E. Bruccoleri, B. D. Olafson, D. J. States, S. Swaminathan, and M. Karplus. *J. Comput. Chem.*, **4, 1983**, 187–217.

(3) Frenkel D, Smit B *Understanding Molecular Simulation* Academic Press: New York **2002**, 64–65.

Table 1: **Icosahedral symmetry operators**[a]

	1	2	3	4	5
1	I (1,1)	F_1 (1,5)	F_2 (1,4)	F_3 (1,3)	F_4 (1,2)
2	**Z** (2,1)	ZF_1 (6,2)	$\underline{ZF_2}$ (11,4)	ZF_3 (9,1)	ZF_4 (5,1)
3	X (3,1)	XF_1 (8,1)	$\overline{XF_2}$ (12,1)	XF_3 (10,4)	XF_4 (7,2)
4	Y (4,1)	YF_1 (4,2)	YF_2 (4,3)	YF_3 (4,4)	YF_4 (4,5)
5	F_1Z (2,5)	$\underline{F_1ZF_1}$ (6,1)	F_1ZF_2 (11,3)	$\mathbf{F_1ZF_3}$ (9,5)	F_1ZF_4 (5,5)
6	$\underline{ZF_1Z}$ (5,2)	$\overline{ZF_1ZF_1}$ (2,2)	ZF_1ZF_2 (6,3)	$\mathbf{ZF_1ZF_3}$ (11,5)	ZF_1ZF_4 (9,2)
7	$\overline{XF_1Z}$ (7,1)	XF_1ZF_1 (3,5)	XF_1ZF_2 (8,5)	XF_1ZF_3 (12,5)	XF_1ZF_4 (10,3)
8	YF_1Z (3,2)	YF_1ZF_1 (8,2)	YF_1ZF_2 (12,2)	YF_1ZF_3 (10,5)	YF_1ZF_4 (7,3)
9	F_2Z (2,4)	F_2ZF_1 (6,5)	F_2ZF_2 (11,2)	$\underline{F_2ZF_3}$ (9,4)	$\mathbf{F_2ZF_4}$ (5,4)
10	ZF_2Z (12,4)	ZF_2ZF_1 (10,2)	ZF_2ZF_2 (7,5)	$\overline{ZF_2ZF_3}$ (3,4)	ZF_2ZF_4 (8,4)
11	XF_2Z (11,1)	XF_2ZF_1 (9,3)	XF_2ZF_2 (5,3)	$\underline{XF_2ZF_3}$ (2,3)	$\mathbf{XF_2ZF_4}$ (6,4)
12	YF_2Z (3,3)	YF_2ZF_1 (8,3)	YF_2ZF_2 (12,3)	$\overline{YF_2ZF_3}$ (10,1)	YF_2ZF_4 (7,4)

[a] Rotational operators of icosahedral symmetry. I is identity; $F_{1,2,3,4}$ are rotations around the 5 fold symmetry axis by 72^0, 144^0, 216^0, 288^0 respectively; X,Y,Z are rotations by 180^0 around X,Y,Z axes respectively. The 1st and 2nd numbers inside the parenthesis following the operator indicates the row and column numbers respectively of the inverse of that operator. Five operators in each row transform the protomer coordinates to 5 protomers for the pentameric primary unit used in this study. Neighboring images of the pentameric unit are generated by the five operators in boldface.

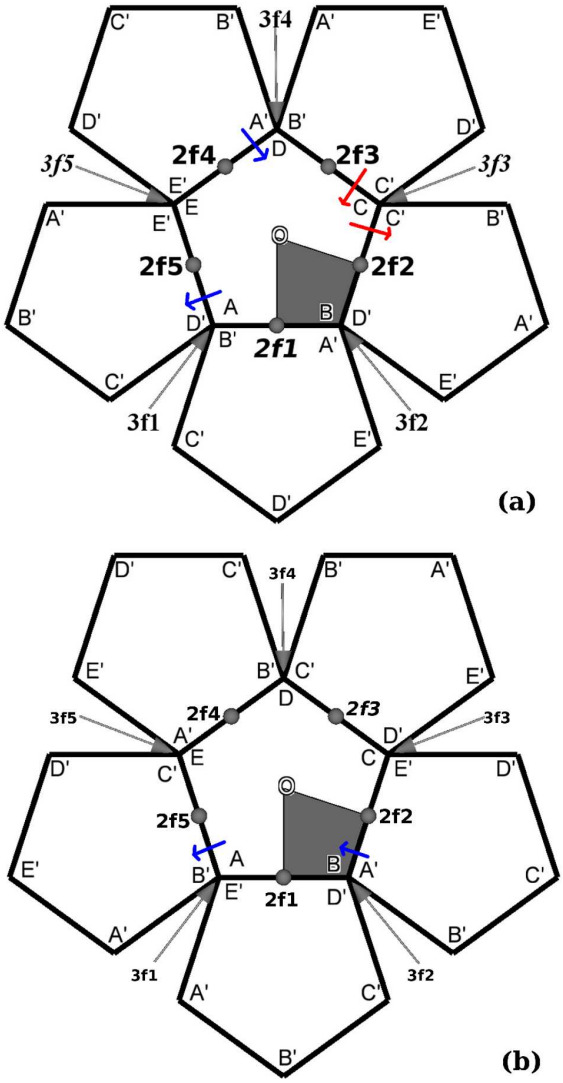

Figure 1: (a) Two-dimensional projection of the pentamer and its neighbors generated by the set of symmetry operators shown in bold face in Table 1. The central pentamer represented by *ABCDE*, is the primary simulation unit. Pentamers represented by $A'B'C'D'E'$ are nearest-neighbor images. The area spanned by a protomer is represented by the shaded area. Three-fold symmetry axes are 3f1 to *3f5* and two-fold symmetry axes are *2f1* to 2f5. *O* is the five-fold symmetry axis. The Z axis is coincident with *2f1*. Self-image and replicate-image interactions are present at one 2-fold symmetry axis, *2f1*, and two 3-fold symmetry axes, *3f3* and *3f5*. (b) Two-dimensional projection of the pentamer and its neighbors generated by the set of underlined symmetry operators in Table 1. Upon recentering an atom might not see an identical micro-environment as this particular choice of symmetry operators does not satisfy the first criterion mentioned in the text.

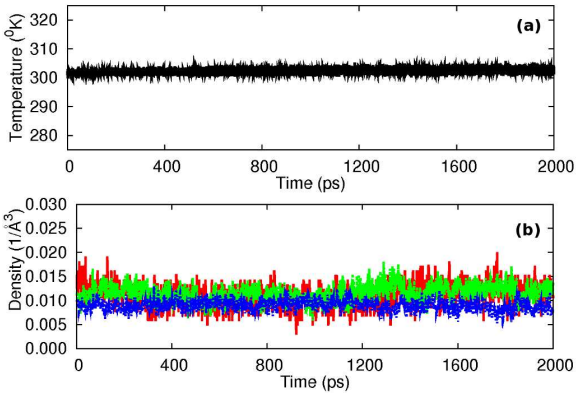

Figure 2: (a) Temprature of solvated viral capsid during 2 ns production period of simulation. (b) Density of heavy atoms of protein within a cylindrical shell of 1 Å width around 3-fold symmetry axis 3f1 with the midpoint of the shell at 5 Å (*red*), 7 Å (*green*) and 9 Å (*blue*).

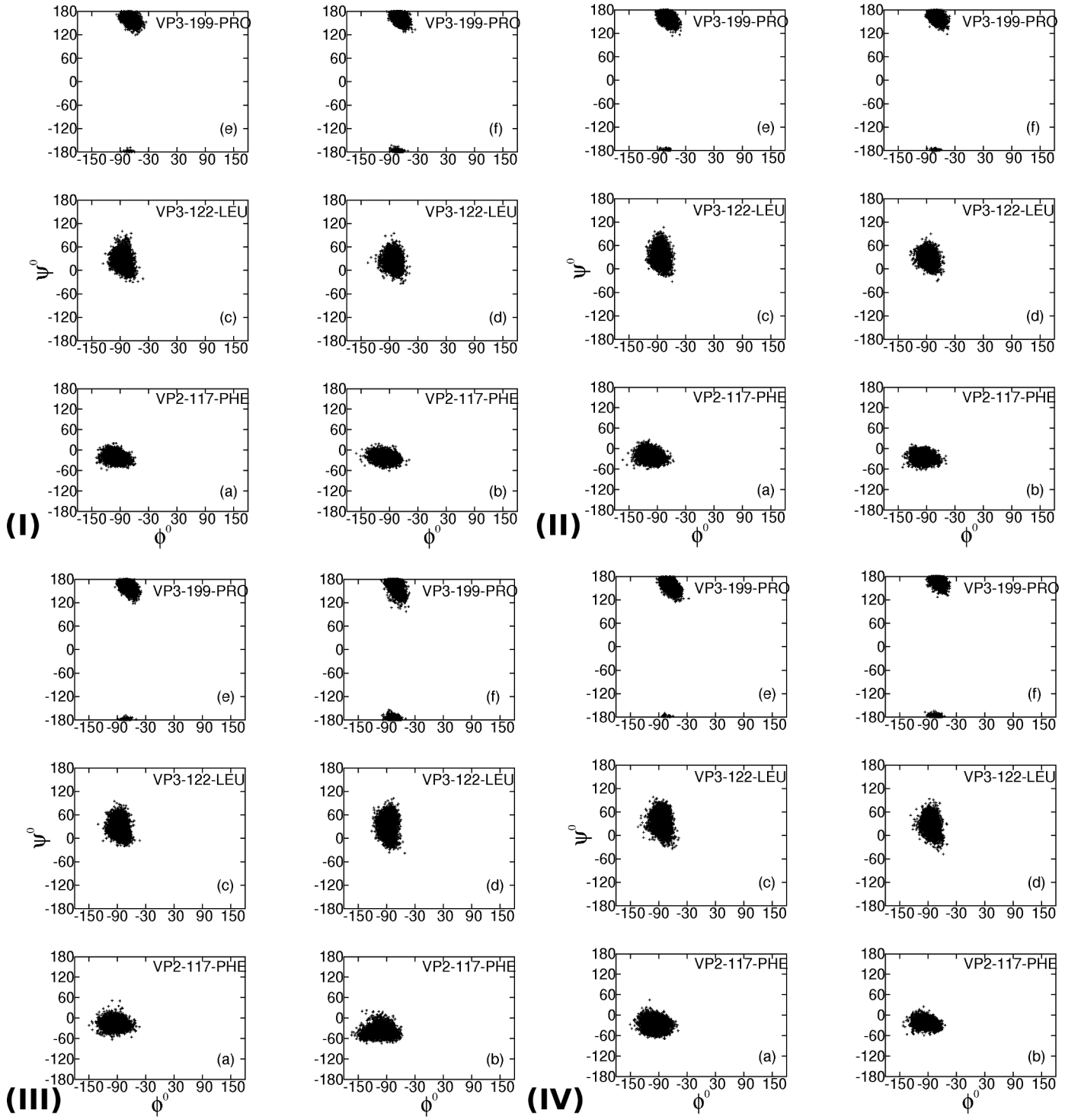

Figure 3: Ramachandran plot of residues closest to 3-fold symmetry axes. The dihedral angles, ϕ and ψ, are plotted for residue 117 of VP2, and residues 122 and 199 of VP3 from protomers located near the 3f1, 3f2 and 3f4 axes (panel *a,c* and *e*), or located near the *3f3* and *3f5* axes (panel *b,d* or *f*). Results are shown for 4 sets of 2 ns production time of simulation - (I), (II), (III) and (IV).